Chinese Journal of Structural Chemistry 45 (2026) 100762

Contents lists available at ScienceDirect

Chinese Journal of Structural Chemistry

journal homepage: www.journals.elsevier.com/chinese-journal-of-structural-chemistry

Article

# Rational design of $ZnIn_2S_4$–COF heterojunction to inhibit photogenerated carrier dynamics for enhanced photocatalytic $CO_2$ reduction

Dongdong Liu[a], Ziqi Tang[a], Haoyu Wang[a], Xinjie Li[a], Jingyang Li[a], Chao Zhu[b], Shan Ding[a], Yuan-Sheng Cheng[a], Hui Zhang[a], Peipei Li[a,*], Ju Wu[a,**], Guozan Yuan[b,***]

[a] School of Materials and Chemical Engineering, Anhui Province Key Laboratory of Conservation and Utilization for Dabie Mountain Special Bio-Resources, West Anhui University, Lu'an, Anhui, 237012, China
[b] School of Chemistry and Chemical Engineering, Anhui University of Technology, Maanshan, 243032, China

ARTICLE INFO

*Keywords:*
Zinc indium sulfide
Covalent organic framework
Heterojunction
Photocatalytic $CO_2$ reduction

ABSTRACT

Using solar energy to convert $CO_2$ into chemicals presents an economical, environmentally friendly, and sustainable approach. However, single-component photocatalysts exhibit limitations, including a narrow light absorption range, rapid carrier recombination, and weak reduction capabilities. To mitigate charge carrier recombination and enhance reduction efficiency, this study prepared heterojunction photocatalysts by *in situ* growing zinc indium sulfide ($ZnIn_2S_4$) on a covalent organic framework (COF) substrate. Under visible light irradiation, the 30% ZIS-COF heterojunction demonstrated the highest $CO_2$ reduction performance (1187.2 μmol $g^{-1}$) and selectivity exceeding 99%, outperforming the single-component system. The electron transfer mechanism and catalytic process were further explored through photoluminescence (PL), time-resolved fluorescence decay spectra, attenuated total reflection Fourier transform infrared spectroscopy, and spin polarized density functional theory (DFT) calculations. The results reveal that, upon photoexcitation, electrons in COF migrate to $ZnIn_2S_4$ (ZIS), and the efficient flow of photoexcited electrons is facilitated by the intimate interface contact between COF and ZIS. Moreover, the porous structure of COF promotes $CO_2$ adsorption and enhances mass transfer. This study establishes a versatile platform for developing various hybrid combinations of $CO_2$-reducing metal semiconductors and photosensitizing COF materials, paving the way for enhanced photocatalytic performance.

## 1. Introduction

The escalating global energy crisis and intensifying environmental challenges have made the development of sustainable technologies for energy conversion and greenhouse gas mitigation a central focus of contemporary scientific research [1]. Among these technologies, solar-driven photocatalytic $CO_2$ reduction has attracted significant attention due to its potential to convert greenhouse gases into valuable chemicals and fuels [2–7], offering substantial promise for reducing carbon emissions and achieving carbon neutrality. However, current photocatalytic systems are often limited by critical issues such as low catalytic efficiency, poor selectivity, and insufficient stability [8–10]. These challenges highlight the pressing need for the rational design of novel photocatalysts with enhanced activity and durability.

Covalent organic frameworks (COFs) are a class of crystalline, porous materials composed of light elements (e.g., C, H, O, N) interconnected through covalent bonds [11–14]. These materials exhibit high specific surface areas, tunable pore sizes, and excellent light-harvesting and charge-transport properties, making them promising candidates for photocatalytic applications in recent years. The ordered π-conjugated structures of COFs promote efficient separation and migration of photoexcited charge carriers, positioning them as an ideal platform for photocatalytic $CO_2$ reduction [15–18]. However, pristine COFs are often limited by low visible-light absorption and high recombination rates of photogenerated electron-hole pairs, which significantly hinder their catalytic performance in practical applications [19,20]. To overcome these limitations, researchers have explored the integration of COFs with semiconductor photocatalysts to form efficient heterojunction

* Corresponding author.
** Corresponding author.
*** Corresponding author.
*E-mail addresses:* lpp0516@126.com (P. Li), lawuju@ustc.edu.cn (J. Wu), guozan@ahut.edu.cn (G. Yuan).

https://doi.org/10.1016/j.cjsc.2025.100762
Received 19 August 2025; Received in revised form 26 September 2025; Accepted 6 October 2025
Available online 11 October 2025

systems, aiming to enhance the separation and transport of photogenerated charge carriers [21,22]. To date, numerous studies have reported the construction of Z- or S-scheme heterojunctions by integrating COFs with various inorganic semiconductors, such as g-$C_3N_4$ [23], $TiO_2$ [24], and CdS [25], achieving significant improvements in photocatalytic performance. Among various candidates, $ZnIn_2S_4$ (ZIS), an n-type semiconductor, has gained considerable attention due to its suitable band gap, strong visible-light absorption, and excellent chemical stability, making it widely studied for photocatalytic reactions under visible light [26–28]. However, ZIS still faces challenges such as rapid recombination of photogenerated charge carriers and a limited number of active catalytic sites. The hybridization of ZIS with COFs offers a promising strategy to synergistically combine their respective advantages, thus creating a highly efficient platform for photocatalytic $CO_2$ reduction. Among the various COF materials reported, nitrogen-rich COFs, such as tris(4-formylphenyl)amine (Tfa) and 2,4,6-tris(4-aminophenyl)triazine (Tta), are particularly promising for $CO_2$ capture due to the increased affinity of nitrogen atoms for $CO_2$ interactions. However, the integration of COFs with ZIS remains in the early stages of development, and our understanding of the structural design, interfacial engineering, and underlying photocatalytic mechanisms of such hybrid systems is still limited. Therefore, a comprehensive investigation into the construction strategies of ZIS-COF heterojunctions, along with a deeper exploration of the relationship between their structure and photocatalytic behavior in $CO_2$ reduction reactions, is crucial for advancing high-efficiency artificial photosynthesis technologies [29,30].

In this study, we selected Tfa and Tta as precursors for the synthesis of a COF via Schiff-base condensation, and constructed a novel ZIS-COF heterojunction photocatalyst. By optimizing the synthesis method and interfacial design, we systematically investigated the photocatalytic performance of the heterojunction for $CO_2$ reduction. The 30% ZIS-COF exhibited the highest CO yield of 1187.2 μmol $g^{-1}$, with an outstanding selectivity of 99%. The enhanced photocatalytic performance of ZIS-COF can be attributed to the incorporation of COF, which introduces triazine units as visible light absorbers and establishes a layered heterostructure, facilitating close interface interactions and enhanced charge transfer. Additionally, the reaction mechanism was elucidated through a combination of morphological characterization, photoluminescence (PL), time-resolved fluorescence decay spectra, spin-polarized density functional theory (DFT) calculations, and *in situ* spectroscopic analyses. These findings are expected to provide valuable theoretical insights and experimental guidance for the rational design and development of advanced organic-inorganic photocatalytic materials.

## 2. Results and discussion

The synthesis route of ZIS-COF is illustrated in Scheme 1. Initially, the COF was synthesized using Tfa and Tta as the starting materials, followed by the *in-situ* growth of ZIS on the COF surface. As shown in Fig. 1(a), pure COF exhibits typical diffraction peaks at 4.5°, 7.7°, and 11.8°, indicating its highly ordered crystalline structure [31]. Pure ZIS displays characteristic diffraction peaks at 21.2°, 27.6°, 47.2°, and 52.4°, corresponding to the (006), (102), (110), and (116) crystal planes [32], respectively (JCPDS 65–2023). The PXRD pattern of ZIS-COF contains both the characteristic peaks of COF and ZIS, with no significant impurity peaks, suggesting successful integration of the two materials without compromising their respective crystal structures. SEM images reveal that COF exhibits an irregular, porous block structure, while ZIS adopts a flower-like nanosheet morphology with an approximate size of 500–600 nm (Fig. S1). In the ZIS-COF, ZIS uniformly grows on the surface of COF, forming a tightly integrated heterojunction interface (Fig. 1(b)). HRTEM further confirms the intimate contact between ZIS and COF (Fig. 1(c) and Fig. S2). Specifically, the (102) interplanar spacing of ZIS is 0.32 nm [33], while COF shows amorphous characteristics, with a distinct interface between the two materials. Fig. 1(d) displays high-angle annular dark field (HAADF) images and energy-dispersive X-ray spectroscopy (EDS) elemental mapping of the ZIS-COF, revealing a uniform distribution of C, N, Zn, In and S throughout the structure. The chemical stability of ZIS-COF was assessed by PXRD analysis after treatment in various solvents, including 1 M NaOH, DMF, MeOH, MeCN, water and boiling water for 24 h (Fig. S3). The ZIS-COF demonstrated robust stability in all these solvents, as evidenced by nearly unchanged PXRD patterns.

XPS measurements were conducted to investigate the surface chemistry of pristine COF, ZIS and 30% ZIS-COF heterojunction (Fig. S4–5). As shown in Fig. 2(a), the XPS survey spectrum confirms the presence of C, N, Zn, In and S elements in 30% ZIS-COF, verifying the successful synthesis of the heterojunction material. In Fig. 2(b), the fitted peaks at 284.0 and 285.2 eV are attributed to the C–C and C=N bonds in COF, respectively. The N 1s peak at 397.6 eV corresponds to the C=N–C bonds in the COF (Fig. 2(c)). The high-resolution Zn 2p spectrum

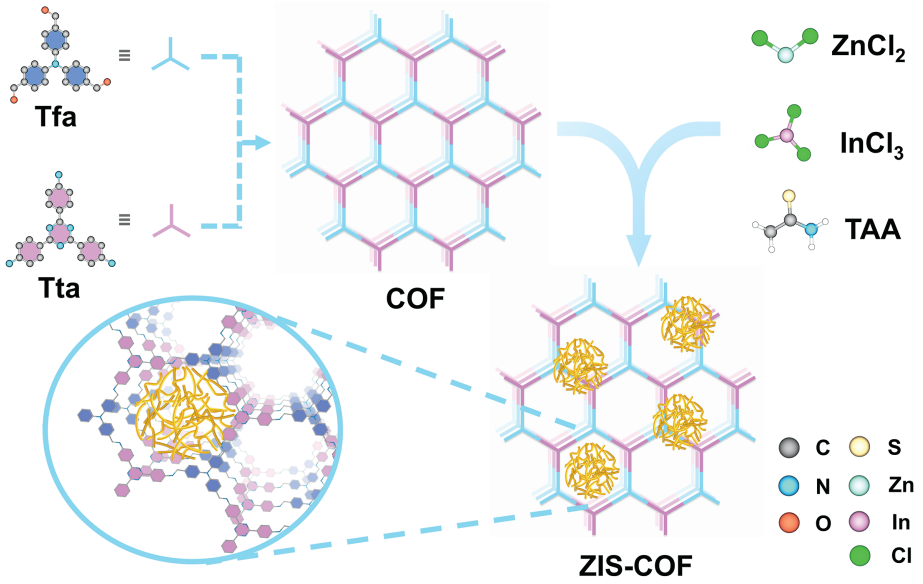


**Scheme 1.** Schematic synthesis process of ZIS-COF.

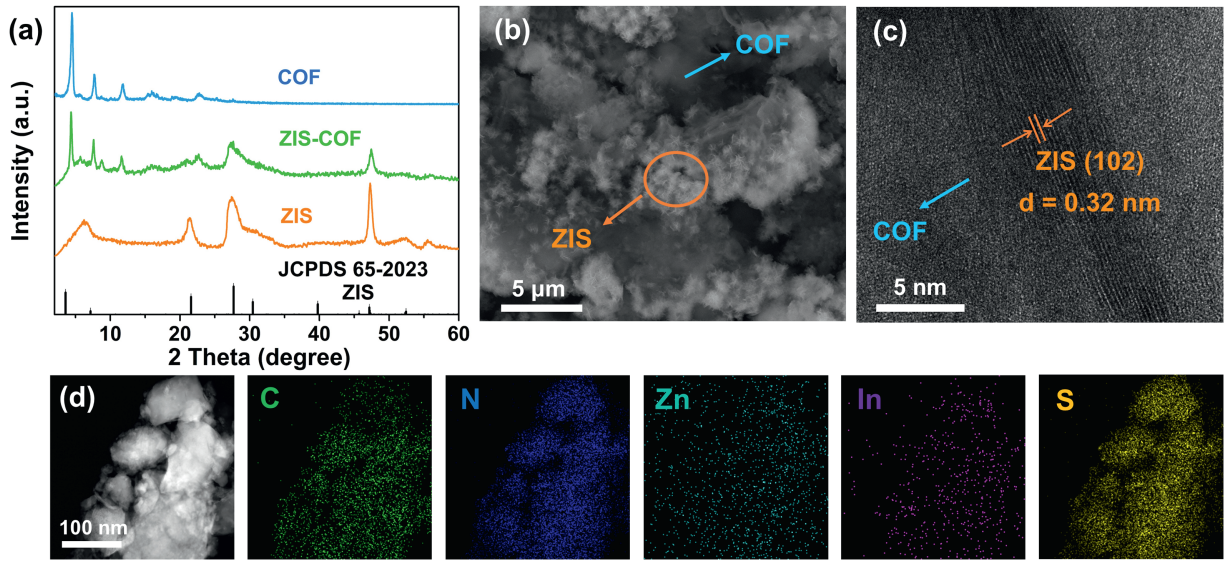


**Fig. 1.** (a) XRD patterns of COF, ZIS and ZIS-COF. (b) SEM images of ZIS-COF. (c) HRTEM image of ZIS-COF. (d) HAADF-STEM image and EDX mapping images of ZIS-COF.

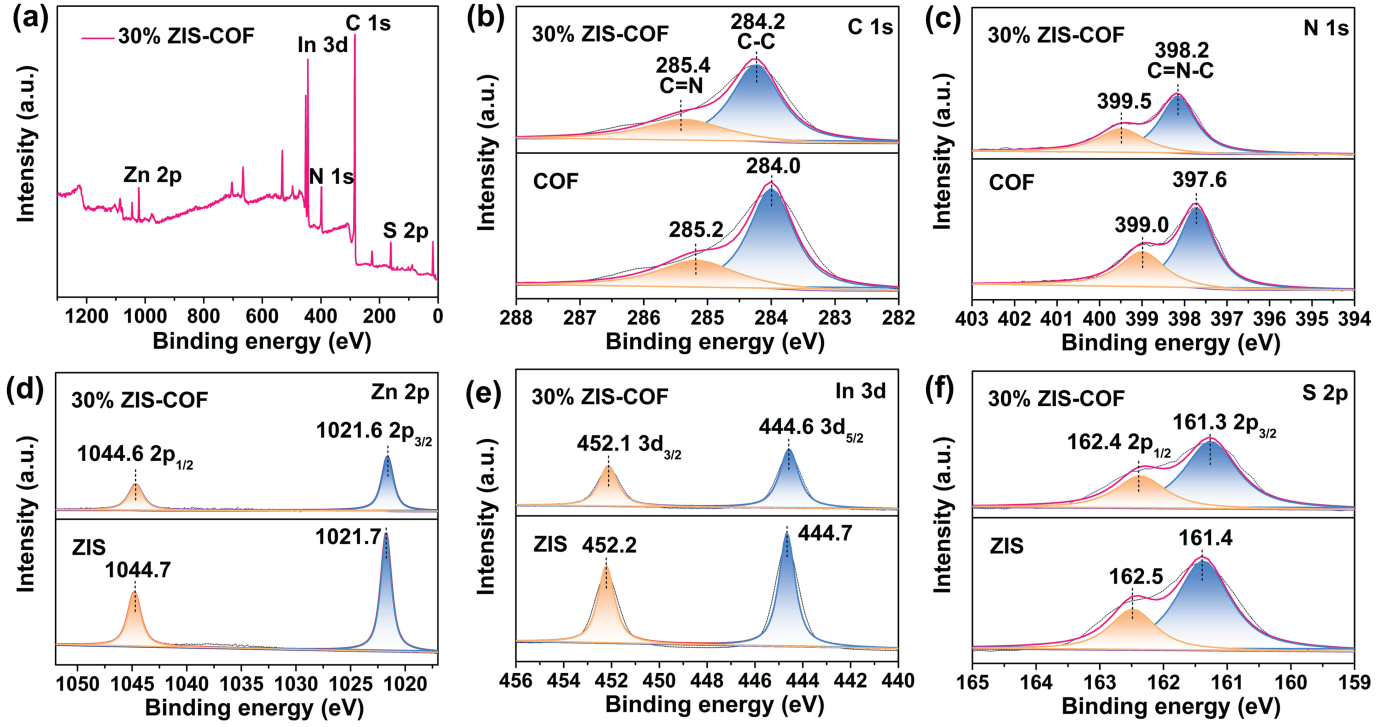


**Fig. 2.** (a) XPS survey spectrum of 30% ZIS-COF. High-resolution XPS spectra of COF, ZIS and 30% ZIS-COF: (b) C 1s, (c) N 1s, (d) Zn 2p, (e) In 3d, and (f) S 2p.

(Fig. 2(d)) reveals binding energies at 1021.7 eV (Zn $2p_{3/2}$) and 1044.7 eV (Zn $2p_{1/2}$), consistent with the $Zn^{2+}$ oxidation state [34]. The peaks at 444.7 eV (In $3d_{5/2}$) and 452.2 eV (In $3d_{3/2}$) in the In 3d spectrum (Fig. 2(e)) indicate the presence of $In^{3+}$ [35]. Compared to pure ZIS, the binding energies of Zn 2p and In 3d in the ZIS-COF heterojunction are both shifted to lower values, suggesting electron transfer from COF to ZIS. In Fig. 2(f), the peaks at 161.4 and 162.5 eV, assigned to the $2p_{3/2}$ and $2p_{1/2}$ states of S, respectively, are characteristic of $S^{2-}$ and are consistent with reported values in the literature [36].

To evaluate the potential application of ZIS, COF, and ZIS-COF composites in photocatalytic $CO_2$ reduction, a series of photophysical property analyses were performed. First, the $CO_2$ adsorption capacity was tested. The results show that the $CO_2$ adsorption amounts of COF at room temperature are 35.0 $cm^3\ g^{-1}$, exhibiting relatively high $CO_2$ adsorption capacities (Fig. S6). Although the $CO_2$ adsorption capacities of all the heterojunction are slightly reduced compared to pure COF, the 30% ZIS-COF still demonstrates a high $CO_2$ adsorption capacity of 17.3 $cm^3\ g^{-1}$. Furthermore, the bandgap ($E_g$) of a photocatalyst is crucial for determining charge carrier transport and separation pathways. UV-vis diffuse reflectance spectroscopy (DRS) measurements reveal that the absorption edge of ZIS is approximately 450 nm (bandgap-2.41 eV), while COF exhibits strong absorption in the visible light region (Fig. S6–7). The absorption edge of the ZIS-COF heterojunction is red-shifted to 600 nm, indicating that the introduction of COF enhances its

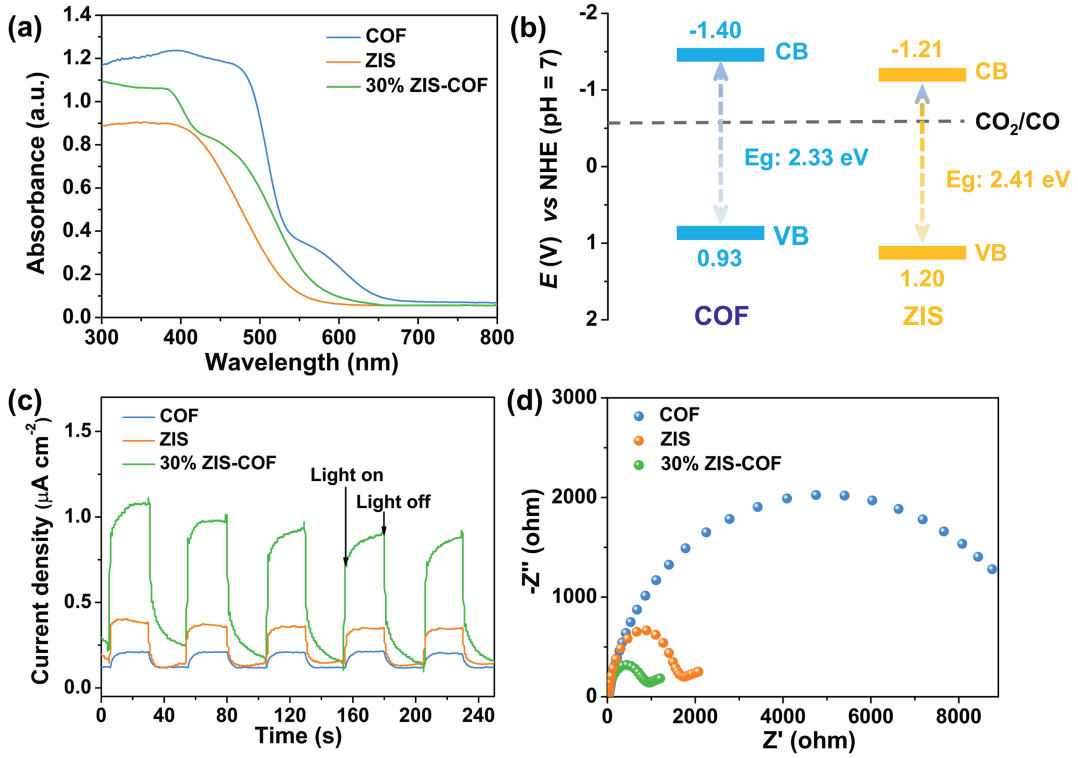


**Fig. 3.** (a) Solid-state UV-vis absorption spectra of COF, ZIS and 30% ZIS-COF. (b) Band-structure diagram for COF and ZIS. (c) Transient photocurrent responses and (d) EIS spectra of COF, ZIS and 30% ZIS-COF.

visible light capture capability (Fig. 3(a)). Mott-Schottky measurements confirmed that COF and ZIS both are n-type semiconductors (Fig. S8–9), with flat band potentials of −1.60 and −1.41 V, respectively, allowing determination of the conduction band and valence band positions. As shown in Fig. 3(b), the lowest unoccupied molecular orbitals (LUMOs) of ZIS and COF are more negative than the standard reduction potential of $CO_2$/CO, suggesting that the heterojunction can effectively couple with $CO_2$ reduction. Transient photocurrent response experiments revealed that 30% ZIS-COF exhibited significantly higher photocurrent than either of the individual components, confirming that the ZIS-COF heterojunction enhances electron transfer (Fig. 3(c)). Additionally, electrochemical impedance spectroscopy (EIS) measurements showed that compared to individual ZIS and COF components, 30% ZIS-COF exhibited the smallest semicircle diameter in the Nyquist plot,

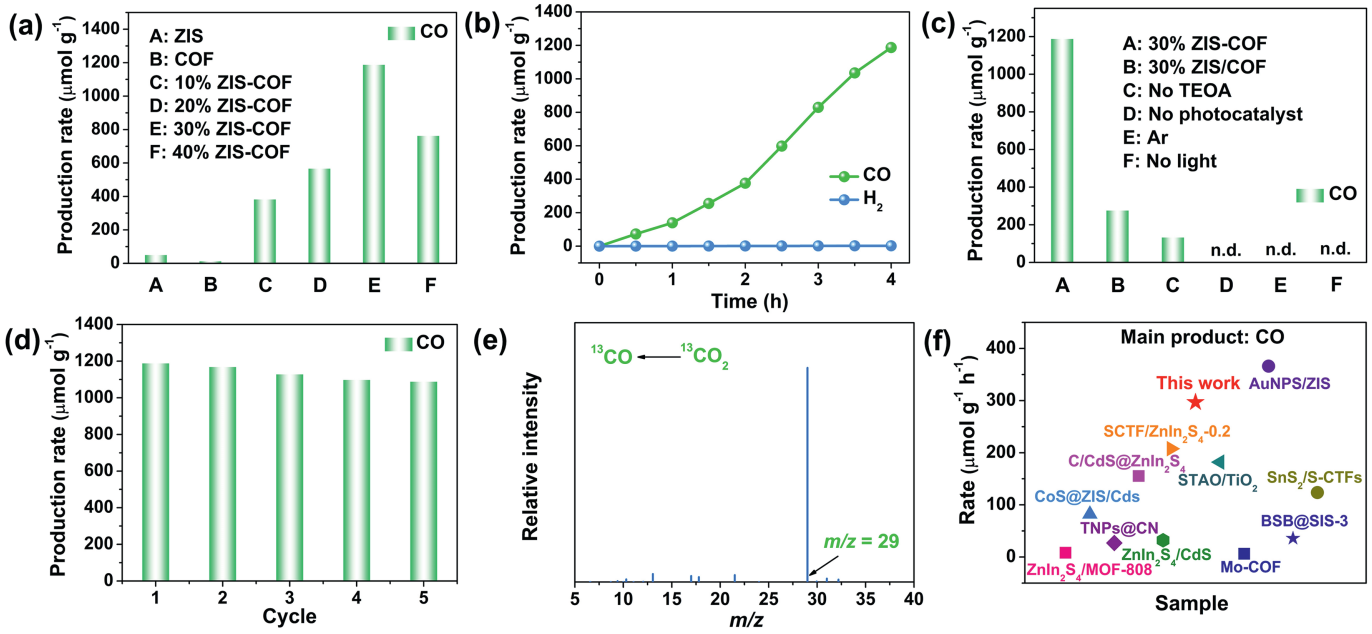


**Fig. 4.** (a) Results of photocatalysis of different photocatalysts. (b) Time-dependent CO and $H_2$ production performance using 30% ZIS-COF as photocatalyst. (c) Photocatalytic performances of various catalysts and conditions. (d) Recycle activity stability test of 30% ZIS-COF in $CO_2$ photoreduction. (e) Mass spectrum of the products from the photocatalytic reduction of $^{13}CO_2$ using 30% ZIS-COF as photocatalyst. (f) Comparison of photocatalytic $CO_2$ reduction performance with recently reported photocatalysts.

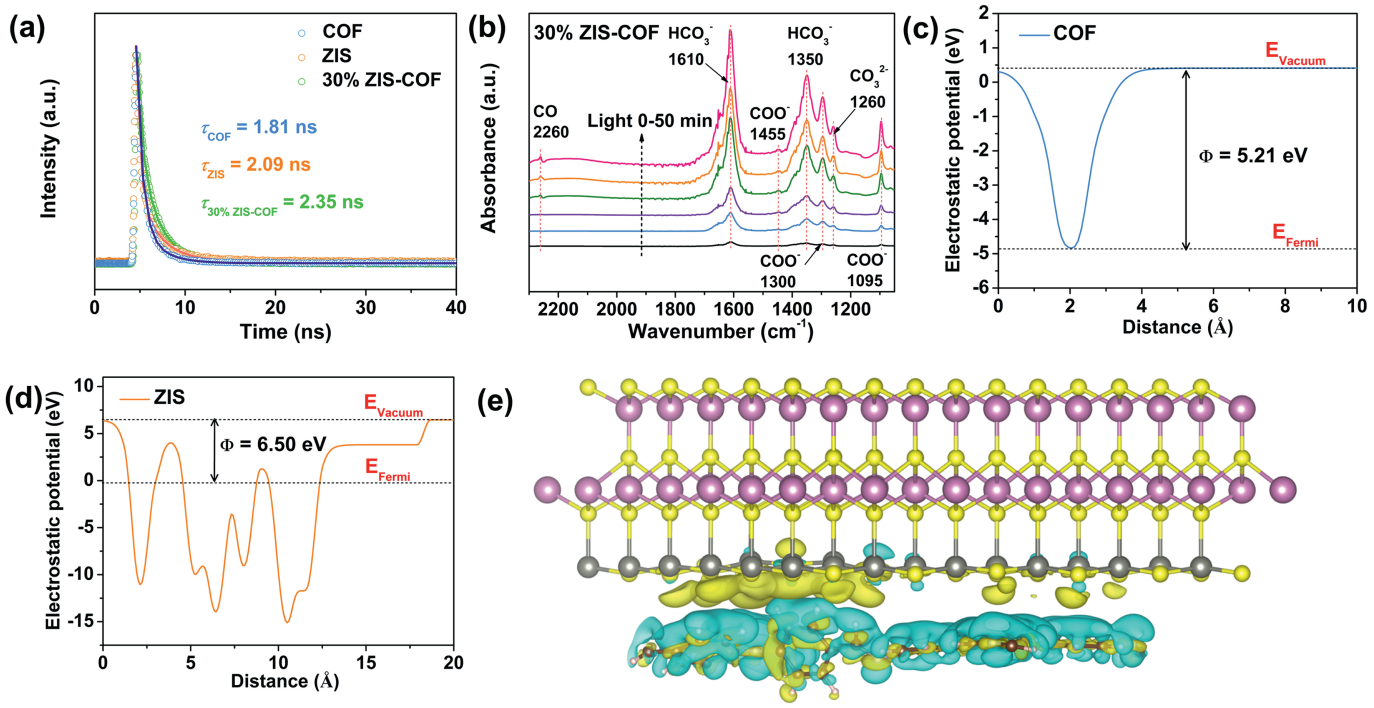


**Fig. 5.** (a) Time-resolved transient PL decay of COF, ZIS and 30% ZIS-COF. (b) *In situ* ATR-IFTS spectra for $CO_2$ photoreduction over 30% ZIS-COF. DFT calculation of the COF and ZIS structure. Electrostatic potential along the *z* axis of COF (c) and ZIS (d) interface. (e) The electron density distribution of ZIS-COF interface. Yellow and blue clouds denote electron increasing and reducing area, respectively.

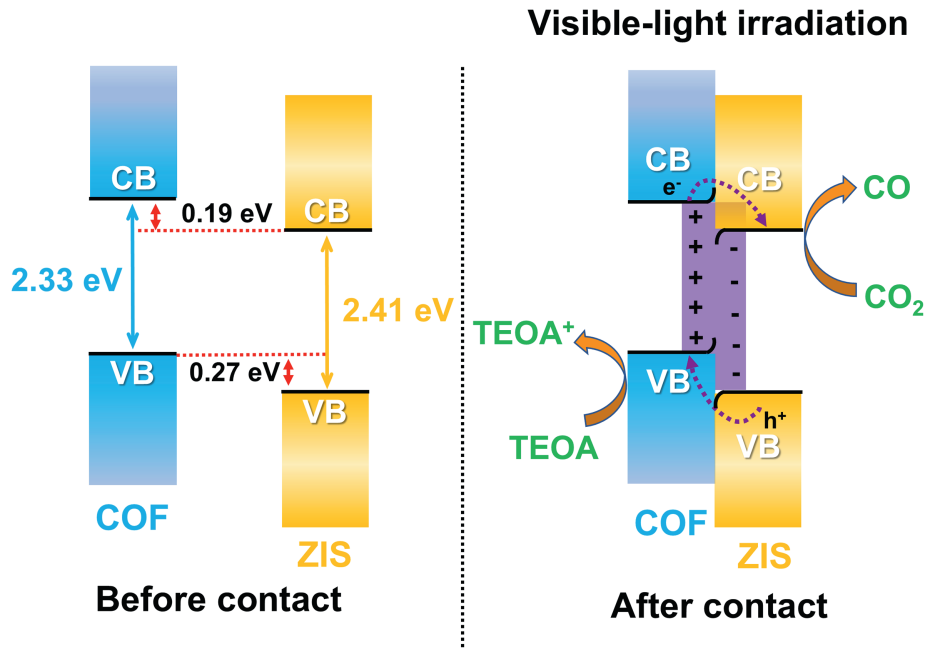


**Fig. 6.** Proposed reaction mechanism for photocatalytic $CO_2$ reduction on the ZIS-COF heterojunction.

indicating the lowest charge transfer resistance at the interface (Fig. 3 (d)). These results further highlight that the ZIS-COF heterojunction effectively enhances charge transfer.

The photocatalytic $CO_2$ reduction performance was conducted on the prepared catalyst under visible-light illumination in a $CO_2$-saturated $H_2O$ solution, without the addition of any photosensitizer. As shown in Fig. 4(a), pure ZIS only produces 50.0 μmol $g^{-1}$ of CO after 4 h of reaction, while pure COF exhibits lower catalytic activity, yielding only 12.5 μmol $g^{-1}$. Notably, the ZIS-COF heterojunctions show significantly enhanced catalytic performance, with the optimal 30% ZIS-COF achieving a CO yield of 1187.2 μmol $g^{-1}$, which is 95 times higher than that of pure COF. In contrast, the 40% ZIS-COF sample exhibited a significantly lower CO evolution rate of 762.4 μmol $g^{-1}$ (Table S1). Excessive ZIS loading may cover the surface of COF, thereby diluting the visible-light driven agent. This performance surpasses previously reported $CO_2$ photoreduction catalysts (Fig. 4(f) and Table S4). Meanwhile, the production of by-products of $H_2$ was effectively suppressed below 2.2 μmol $g^{-1}$ (Table S3), demonstrating that the heterojunction

structure promotes selective reduction of $CO_2$. The performance of the 30% ZIS-COF catalyst was also examined over varying irradiation times (Fig. 4(b) and Table S2), with CO release slowing down and plateauing after approximately 4 h. Control experiments were conducted to evaluate the individual components of the 30% ZIS-COF heterojunction, only the 30% ZIS-COF composite exhibited significant photocatalytic activity (Fig. 4(c)), highlighting the advantages of heterostructure. No liquid-phase products were detected by $^1$H NMR analysis. Moreover, the 30% ZIS-COF catalyst exhibited excellent durability over five cycles, with only minimal performance decay (Fig. 4(d)). PXRD, HRTEM and XPS analyses confirmed that the crystallinity and structural integrity of the catalyst were retained after the reaction (Fig. S10–12). To verify the carbon source of generated CO, the $^{13}$C isotopic labeling experiment was performed using $^{13}CO_2$. As shown in Fig. 4(e), the MS peak at $m/z = 29$, corresponding to $^{13}$CO, confirmed that the CO products originated from $CO_2$ rather than other carbon sources. These results collectively demonstrate that ZIS-COF is an efficient and selective heterogeneous photocatalyst capable of achieving $CO_2$ photoreduction.

The recombination behavior of photogenerated charge carriers was studied using PL and time-resolved photoluminescence (TR-PL) spectroscopy. Compared to individual COF components, the fluorescence intensity of the heterojunction materials was significantly reduced to varying degrees (Fig. S13), with the 30% ZIS-COF exhibiting the weakest fluorescence intensity. This reduction indicates that the ZIS-COF heterojunction effectively suppresses the recombination of photoinduced electrons and holes, thus promoting efficient electron transfer. The results of TR-PL revealed that the heterojunction materials exhibited longer fluorescence lifetime compared to pure COF and ZIS (Fig. 5(a)), with the 30% ZIS-COF showing the longest fluorescence lifetime of 2.35 ns. This indicates that the photogenerated charge carriers can effectively migrate between COF and ZIS. This result is consistent with the fluorescence quenching observed in the PL, further confirming that the heterojunction interface promotes the separation of photogenerated electron-hole pairs.

Moreover, *in situ* diffuse reflectance infrared Fourier transform spectroscopy (DRIFTS) was employed to investigate reaction intermediates (Fig. 5(b)). As the irradiation time increased from 0 to 50 min, several species were observed in the reaction process, including bicarbonate species ($HCO_3^-$, 1350 and 1610 cm$^{-1}$) and carbonate species ($CO_3^{2-}$, 1260 cm$^{-1}$), revealing that the presence of absorbed $CO_2$ and dissociated $H_2O$ molecules on the surface of 30% ZIS-COF [37]. The characterization peaks at 1095, 1300 and 1455 cm$^{-1}$ were attributed to $COO^-$ species, which are widely recognized as key intermediates in the conversion of $CO_2$ to CO [38]. Meanwhile, the peaks at 2260 cm$^{-1}$, corresponding to CO, gradually increased with prolonged illumination, further suggesting that CO is primarily produced from the consumption of the $COO^-$ intermediate, confirming the reaction pathway of $CO_2 \rightarrow COOH \rightarrow CO$ [39]. Additionally, spin polarized DFT calculations were employed to gain further insights into the photogenerated charge separation and migration at the COF and ZIS interface (Fig. S14–16). The work function (WF) values of COF and ZIS were found to be 5.21 and 6.50 eV, respectively (Fig. 5(c−d)). The electrostatic potential of ZIS was higher than that of COF, leading to the formation of an interfacial electrical field and Schottky barrier. These findings indicate that electrons are driven to migrate from COF to ZIS due to the WF difference, resulting in an increased electron density on the ZIS side and a decreased electron density on the COF side. Furthermore, simulations of the heterojunction interface between COF and ZIS demonstrated that electrons migrate from COF to ZIS, effectively separating from the holes (Fig. 5(e)). Additionally, we have provided the theoretical adsorption capacities of COF and ZIS for $CO_2$, which are −0.16 and −0.37 eV, respectively (Fig. S17). This suggests that both ZIS and COF demonstrate good $CO_2$ adsorption capacity after forming a heterojunction, which is advantageous for photocatalytic $CO_2$ reduction.

Based on the above results, we propose a mechanism for photocatalytic $CO_2$ reduction in the heterojunction (Fig. 6). COF function serves a dual role as both a $CO_2$ adsorbent and a photosensitizer, absorbing photons to induce the HOMO-to-LUMO transition under visible-light irradiation. The photogenerated electron-hole pairs in the excited COF can migrate and separate at the interface with ZIS due to interfacial interactions. Consequently, $CO_2$ reduction primarily occurs at the catalytic sites on ZIS rather than that on COF. This electron transfer not only significantly inhibits recombination of the excited COF but also shortens the charge transfer distance, thereby boosting photocatalytic efficiency. It can be concluded that the *in-situ* integration of ZIS-COF proves highly effective in dramatically improving visible-light-driven $CO_2$ conversion efficiency.

## 3. Conclusion

In summary, we have rationally designed and fabricated a series of ZIS-COF heterojunction photocatalysts through *in-situ* growth, achieving efficient photocatalytic $CO_2$ reduction reaction. The 30% ZIS-COF exhibited the highest CO production rate of 1187.2 μmol g$^{-1}$. The electron transfer mechanism was further validated by *in situ* spectroscopic analyses and DFT calculations, which confirmed that the heterojunction effectively inhibits the recombination of photogenerated charge carriers and promotes $CO_2$ activation through charge transfer. This study provides both experimental and theoretical insights for the application of ZIS-COF heterojunctions in photocatalytic $CO_2$ reduction and offers a new perspective for designing efficient and stable organic-inorganic composite photocatalysts. Future work could focus on optimizing the functional groups and pore structures of COFs or incorporating co-catalysts to enhance product diversity and reaction efficiency.

## CRediT authorship contribution statement

**Dongdong Liu:** Writing – review & editing, Writing – original draft, Formal analysis, Data curation, Conceptualization. **Ziqi Tang:** Formal analysis, Data curation. **Haoyu Wang:** Formal analysis, Data curation. **Xinjie Li:** Methodology, Funding acquisition. **Jingyang Li:** Methodology, Data curation. **Chao Zhu:** Data curation, Investigation. **Shan Ding:** Methodology, Investigation, Conceptualization. **Yuan-Sheng Cheng:** Writing – review & editing, Methodology. **Hui Zhang:** Methodology, Funding acquisition. **Peipei Li:** Writing – review & editing, Data curation. **Ju Wu:** Writing – review & editing, Software, Resources. **Guozan Yuan:** Writing – review & editing, Resources, Project administration, Methodology.

## Data availability

The data that have been used are confidential.

## Declaration of competing interest

The authors declare that they have no known competing financial interests or personal relationships that could have appeared to influence the work reported in this paper.

## Acknowledgements

This work was supported by the National Natural Science Foundation of China (22171002 and 21603001), the Wanjiang Scholar Program, West Anhui University High Level Talent Research Launch Project (WGKQ2021003), the Excellent Research and Innovation Team Project of Anhui Province (2023AH010077), Natural Science Youth Project of West Anhui University (WXZR202411), Key Project of Education Department of Anhui Province (2024AH052001), Key Research and Development Project of Anhui Province (2024AH051985), Excellent Youth Research Project of Education Department of Anhui Province (YQYB2024053), Open Research Fund Program of Anhui Provincial International Joint Research Center of Modern Environmental Engineering, Anhui University of Science and Technology

(XDHJGC2024009), West Anhui University Natural Science Research Project (WXZR202411), and West Anhui University High level Talent Research Launch Fund Support Project (WGKQ2025004).

## Appendix A. Supplementary data

Supplementary data to this article can be found online at https://doi.org/10.1016/j.cjsc.2025.100762.

## References


[1] S. Davoodi, M. Al-Shargabi, D.A. Wood, V.S. Rukavishnikov, K.M. Minaev, Review of technological progress in carbon dioxide capture, storage, and utilization, Gas Sci. Eng. 117 (2023) 205070, https://doi.org/10.1016/j.jgsce.2023.205070.

[2] J. Ma, L. Li, Y. Zhang, J. Qian, X. Wang, Covalent organic frameworks: synthesis, structures, characterizations and progress of photocatalytic reduction of $CO_2$, Chin. J. Struct. Chem. 43 (2024) 100466, https://doi.org/10.1016/j.cjsc.2024.100466.

[3] D. Lee, K. Yamauchi, K. Sakai, Water-induced switching in selectivity and steric control of activity in photochemical $CO_2$ reduction catalyzed by RhCp*(bpy) derivatives, J. Am. Chem. Soc. 146 (2024) 31597–31611, https://doi.org/10.1021/jacs.4c09486.

[4] C. Zhu, C. Gong, D. Cao, L.-L. Ma, D. Liu, L. Zhang, Y. Li, Y. Peng, G. Yuan, Cobalt-metalated 1D perylene diimide carbon-organic framework for enhanced photocatalytic $\alpha$-C($sp^3$)-H activation and $CO_2$ reduction, Angew. Chem. Int. Ed. 64 (2025) e202504348, https://doi.org/10.1002/anie.202504348.

[5] X. Li, J. Yu, M. Jaroniec, X. Chen, Cocatalysts for selective photoreduction of $CO_2$ into solar fuels, Chem. Rev. 119 (2019) 3962–4179, https://doi.org/10.1021/acs.chemrev.8b00400.

[6] X. Zhang, P. Wang, X. Lv, X. Niu, X. Lin, S. Zhong, D. Wang, H. Lin, J. Chen, S. Bai, Stacking engineering of semiconductor heterojunctions on hollow carbon spheres for boosting photocatalytic $CO_2$ reduction, ACS Catal. 12 (2022) 2569–2580, https://doi.org/10.1021/acscatal.1c05401.

[7] L. Zhang, J. Liu, Y.-Q. Lan, Hetero-motif molecular junction photocatalysts: a new frontier in artificial photosynthesis, Acc. Chem. Res. 57 (2024) 870–883, https://doi.org/10.1021/acs.accounts.1023c00751.

[8] D. Liu, H. Ma, C. Zhu, F. Qiu, W. Yu, L.-L. Ma, X.-W. Wei, Y.-F. Han, G. Yuan, Molecular Co-catalyst confined within a metallacage for enhanced photocatalytic $CO_2$ reduction, J. Am. Chem. Soc. 146 (2024) 2275–2285, https://doi.org/10.1021/jacs.3c14254.

[9] R. Chen, Z. Ren, Y. Liang, G. Zhang, T. Dittrich, R. Liu, Y. Liu, Y. Zhao, S. Pang, H. An, C. Ni, P. Zhou, K. Han, F. Fan, C. Li, Spatiotemporal imaging of charge transfer in photocatalyst particles, Nature 610 (2022) 296–301, https://doi.org/10.1038/s41586-41022-05183-41581.

[10] J. Lv, J. Xie, A.G.A. Mohamed, X. Zhang, Y. Feng, L. Jiao, E. Zhou, D. Yuan, Y. Wang, Solar utilization beyond photosynthesis, Nat. Rev. Chem 7 (2023) 91–105, https://doi.org/10.1038/s43586-43023-00243-w.

[11] D. Zhou, Q. Chen, J. Zhang, T. Wang, Z.-Q. Liu, Ether-embedded covalent organic frameworks enable efficient photocatalytic $CO_2$ reduction, Angew. Chem. Int. Ed. 64 (2025) e202500329, https://doi.org/10.1002/anie.202500329.

[12] L. Deng, W. Chen, G. Zhou, Y. Liu, L. Liu, Y. Han, Z. Huang, D. Jiang, Synthesis of single-crystal two-dimensional covalent organic frameworks and uncovering their hidden structural features by three-dimensional electron diffraction, J. Am. Chem. Soc. 146 (2024) 35427–35437, https://doi.org/10.1021/jacs.4c14535.

[13] X. Zhang, S. Fu, L. Jia, B. Hou, Y. Cui, Y. Liu, Amplifying chirality-induced spin selectivity in helical covalent organic frameworks through fullerene encapsulation, J. Am. Chem. Soc. 147 (2025) 26546–26556, https://doi.org/10.1021/jacs.5c06460.

[14] Y. Wu, H. Lv, X. Wu, Design of two-dimensional porous covalent organic framework semiconductors for visible-light-driven overall water splitting: a theoretical perspective, Chin. J. Struct. Chem. 43 (2024) 100375, https://doi.org/10.1016/j.cjsc.2024.100375.

[15] R. Shah, S. Ali, F. Raziq, S. Ali, P.M. Ismail, S. Shah, R. Iqbal, X. Wu, W. He, X. Zu, A. Zada, Adnan, F. Mabood, A. Vinu, S.H. Jhung, J. Yi, L. Qiao, Exploration of metal organic frameworks and covalent organic frameworks for energy-related applications, Coord. Chem. Rev. 477 (2023) 214968, https://doi.org/10.1016/j.ccr.2022.214968.

[16] N. Keller, T. Bein, Optoelectronic processes in covalent organic frameworks, Chem. Soc. Rev. 50 (2021) 1813–1845, https://doi.org/10.1039/D0CS00793E.

[17] Y. Liu, C.C.L. McCrory, Modulating the mechanism of electrocatalytic $CO_2$ reduction by cobalt phthalocyanine through polymer coordination and encapsulation, Nat. Commun. 10 (2019) 1683, https://doi.org/10.1038/s41467-41019-09626-41468.

[18] C.-C. Li, M.-Y. Gao, X.-J. Sun, H.-L. Tang, H. Dong, F.-M. Zhang, Rational combination of covalent-organic framework and nano $TiO_2$ by covalent bonds to realize dramatically enhanced photocatalytic activity, Appl. Catal. B Environ. 266 (2020) 118586, https://doi.org/10.111016/j.apcatb.112020.118586.

[19] P. Pachfule, A. Acharjya, J. Roeser, T. Langenhahn, M. Schwarze, R. Schomäcker, A. Thomas, J. Schmidt, Diacetylene functionalized covalent organic framework (COF) for photocatalytic hydrogen generation, J. Am. Chem. Soc. 140 (2018) 1423–1427, https://doi.org/10.1021/jacs.7b11255.

[20] X.-M. Yuan, D.-M. Fei Xiao, C.-L. Zhao, C.-L. Zhang, Enhancing photocatalytic $CO_2$RR by modulating the active sites of COF-based catalysts, Small 21 (2025) 2411316, https://doi.org/10.1002/smll.202411316.

[21] S. Wang, M. Xu, T. Peng, C. Zhang, T. Li, I. Hussain, J. Wang, B. Tan, Porous hypercrosslinked polymer-$TiO_2$-graphene composite photocatalysts for visible-light-driven $CO_2$ conversion, Nat. Commun. 10 (2019) 676, https://doi.org/10.1038/s41467-019-08651-x.

[22] Y. Zhou, P. Dong, J. Liu, B. Zhang, B. Zhang, X. Xi, J. Zhang, Functional groups-dependent Tp-based COF/$MgIn_2S_4$ S-scheme heterojunction for photocatalytic hydrogen evolution, Adv. Funct. Mater. 35 (2025) 2500733, https://doi.org/10.1002/adfm.202500733.

[23] G. Santos, L. Tian, R. Gonçalves, H. García, L. Rossi, Boosting $CO_2$ photoreduction efficiency of carbon nitride via S-scheme g-$C_3N_4$/$Fe_2TiO_5$ heterojunction, Adv. Funct. Mater. 25 (2025) 2422055, https://doi.org/10.1002/adfm.202422055.

[24] J. Ning, J. Huang, Y. Liu, Y. Chen, Q. Niu, Q. Lin, Y. He, Z. Liu, Y. Yu, L. Li, Alkyl-linked $TiO_2$@COF heterostructure facilitating photocatalytic $CO_2$ reduction by targeted electron transport, Chin. J. Struct. Chem. 43 (2024) 100453, https://doi.org/10.1016/j.cjsc.2024.100453.

[25] M. Zhou, S. Wang, P. Yang, C. Huang, X. Wang, Boron carbon nitride semiconductors decorated with CdS nanoparticles for photocatalytic reduction of $CO_2$, ACS Catal. 8 (2018) 4928–4936, https://doi.org/10.1021/acscatal.8b00104.

[26] M. Li, S. Chen, Y. Wang, J. Zhang, Recent progress in photocatalytic reduction of $CO_2$ by $ZnIn_2S_4$-based heterostructures, ChemistrySelect 9 (2024) e202303865, https://doi.org/10.1002/slct.202303865.

[27] Y. Nie, T. Bo, W. Zhou, H. Hu, X. Huang, H. Wang, X. Tan, L. Liu, J. Ye, T. Yu, Understanding the role of Zn vacancy induced by sulfhydryl coordination for photocatalytic $CO_2$ reduction on $ZnIn_2S_4$, J. Mater. Chem. A 11 (2023) 1793–1800, https://doi.org/10.1039/D2TA08336A.

[28] Y. He, H. Rao, K. Song, J. Li, Y. Yu, Y. Lou, C. Li, Y. Han, Z. Shi, S. Feng, 3D hierarchical $ZnIn_2S_4$ nanosheets with rich Zn vacancies boosting photocatalytic $CO_2$ reduction, Adv. Funct. Mater. 29 (2019) 1905153, https://doi.org/10.1002/adfm.201905153.

[29] R. Xiong, X. Ke, W. Jia, Y. Xiao, B. Cheng, S. Lei, Photothermal-coupled solar photocatalytic $CO_2$ reduction with high efficiency and selectivity on a $MoO_{3-x}$@$ZnIn_2S_4$ core-shell S-scheme heterojunction, J. Mater. Chem. A 11 (2023) 2178–2190, https://doi.org/10.1039/D2TA09255G.

[30] K. Chen, X. Wang, Q. Li, Y.-N. Feng, F.-F. Chen, Y. Yu, Spatial distribution of $ZnIn_2S_4$ nanosheets on g-$C_3N_4$ microtubes promotes photocatalytic $CO_2$ reduction, Chem. Eng. J. 418 (2021) 129476, https://doi.org/10.1016/j.cej.2021.129476.

[31] J. Yang, A. Acharjya, M.-Y. Ye, J. Rabeah, S. Li, Z. Kochovski, S. Youk, J. Roeser, J. Grgneberg, C. Penschke, M. Schwarze, T. Wang, Y. Lu, R. Krol, M. Oschatz, R. Schomcker, P. Saalfrank, A. Thomas, Protonated imine-linked covalent organic frameworks for photocatalytic hydrogen evolution, Angew. Chem. Int. Ed. 60 (2021) 19797–19803, https://doi.org/10.1002/anie.202104870.

[32] Z. Zhang, L. Huang, J. Zhang, F. Wang, Y. Xie, X. Shang, Y. Gu, H. Zhao, X. Wang, *In-situ* constructing interfacial contact $MoS_2$/$ZnIn_2S_4$ heterostructure for enhancing solar photocatalytic hydrogen evolution, Appl. Catal. B Environ. 233 (2018) 112–119, https://doi.org/10.1016/j.apcatb.2018.04.006.

[33] Q. Li, X. Li, M. Zheng, F. Luo, L. Zhang, B. Zhang, B. Jiang, Spatial coupling of photocatalytic $CO_2$ reduction and selective oxidation on covalent triazine framework/$ZnIn_2S_4$ core-shell structures, Adv. Funct. Mater. 35 (2025) 2417279, https://doi.org/10.1002/adfm.202417279.

[34] C.Q. Li, X. Du, S. Jiang, Y. Liu, Z.L. Niu, Z.Y. Liu, S.S. Yi, X.Z. Yue, Constructing direct Z-scheme heterostructure by enwrapping $ZnIn_2S_4$ on CdS hollow cube for efficient photocatalytic $H_2$ generation, Adv. Sci. 9 (2022) 2201773, https://doi.org/10.1002/advs.202201773.

[35] S. Lu, S. Zhang, L. Li, C. Liu, Z. Li, D. Luo, Piezoelectric effect-assisted Z-scheme heterojunction $ZnIn_2S_4$/$BaTiO_3$ for improved photocatalytic reduction of $CO_2$ to CO, Chem. Eng. J. 483 (2024) 149058, https://doi.org/10.1016/j.cej.2024.149058.

[36] X. Jia, Y. Lu, K. Du, H. Zheng, L. Mao, H. Li, Z. Ma, R. Wang, J. Zhang, Interfacial mediation by Sn and S vacancies of p-SnS/n-$ZnIn_2S_4$ for enhancing photocatalytic hydrogen evolution with new scheme of type-I heterojunction, Adv. Funct. Mater. 33 (2023) 2304072, https://doi.org/10.1002/adfm.202304072.

[37] D. Wu, Q. Liang, H. Si, X. Yan, H. Huang, Z. Li, Z. Kang, Self-assembly of a heterogeneous microreactor with carbon dots embedded in Ti-MOF derived $ZnIn_2S_4$/$TiO_2$ microcapsules for efficient $CO_2$ photoreduction, J. Mater. Chem. A 10 (2022) 24519–24528, https://doi.org/10.1039/D2TA07217C.

[38] Y. Ma, X. Yi, S. Wang, T. Li, B. Tan, C. Chen, T. Majima, E.R. Waclawik, H. Zhu, J. Wang, Selective photocatalytic $CO_2$ reduction in aerobic environment by microporous Pd-porphyrin-based polymers coated hollow $TiO_2$, Nat. Commun. 13 (2022) 1400, https://doi.org/10.1038/s41467-022-29102-0.

[39] H. Fan, M. Hu, Y. Duan, L. Zuo, R. Yu, Z. Li, Q. Liu, B. Li, L. Wang, Hollow core-shell heterojunction TAPB-COF@$ZnIn_2S_4$ as highly efficient photocatalysts for carbon dioxide reduction, Chem. Sci. 16 (2025) 2316–2324, https://doi.org/10.1039/d4sc07077a.